CrossMark

ORIGINAL CONTRIBUTION

Evaluation of poly(2-hydroxyethyl methacrylate) and poly(methyl methacrylate)-grafted poly(vinylidene fluoride)-poly(dimethylsiloxane) bilayers for gas separation

B. M. Maher[1,2] · J. Rezaali[1,2] · H. Ghaleh[1,2] · S. Fallahnejad[1,2] · F. Abbasi[1,2] · A. A. Babaluo[3]

Abstract Thin film composites (TFCs) of poly(2-hydroxyethyl methacrylate) (PHEMA) and poly(methyl methacrylate) (PMMA) chain-tethered poly(vinylidene fluoride)-poly(dimethylsiloxane) (PVDF-PDMS) were prepared as a gas separation membrane. PDMS was coated on the PVDF support using a dip coating method. PHEMA and PMMA were then grafted on PVDF-PDMS substrate by atom transfer radical polymerization. The PVDF-PDMS-PHEMA and PVDF-PDMS-PMMA trilayer membranes were studied by attenuated total reflection Fourier transform infrared spectroscopy, scanning electron microscopy, atomic force microscopy, water contact angle measurement, and X-ray photoelectron spectroscopy. The results of separation tests indicated that the CO_2/N_2 selectivity of PVDF-PDMS-PHEMA and PVDF-PDMS-PMMA TFCs increased by ~2 and ~3 times, respectively, compared to the solvent-extracted PVDF-PDMS support.

✉ F. Abbasi
f.abbasi@sut.ac.ir

1. Institute of Polymeric Materials, Sahand University of Technology, Tabriz, Iran

2. Faculty of Polymer Engineering, Sahand University of Technology, Tabriz, Iran

3. Nanostructure Materials Research Center, Chemical Engineering Department, Sahand University of Technology, Tabriz, Iran

Introduction

Most studies on gas separation membranes have used dense homogeneous films. They have important properties, like intrinsic gas diffusivity, solubility, and gas permeability. However, the low flux and poor mechanical resistance restrict the capacity of these thick films in practical industrial implementations [1].

Thin film composite membrane is one of the most effective membranes for gas separation because of its asymmetric and porous structure [2]. The configuration of a composite membrane consists of three layers, namely porous support layer, coating layer, and selective layer [3, 4]. The coated macroporous support is normally modified by the formation of a selective polymer layer [5]. The existence of a thin nonporous selective layer over a support providing sufficient mechanical stability guarantees high membrane permeability [6].

The porous support layer is expected to have a high mechanical strength along with an enhanced gas permeability. The important materials utilized as supporting layer include alumina [7], zeolite [8], polysulfone [9], polyamide [10], and poly(vinylidene fluoride) (PVDF) [9]. The coating layer plugs defects in the selective layer and decreases possibility of gas leakage through the defects. The efficiency of a composite membrane is greatly related to coating material filling the defects during the fabrication [10]. Silicone rubber [11, 12], 4,4′-hexafluoroisopropylidene bis(phthalic anhydride) [13], and poly(aminosiloxane) [14] have been applied as coating layers. The selective top layer must be thin as far as possible to obtain a high flux [15, 16]. Thin polymeric films are not strong enough to endure high gas pressure involved in gas separation [16]. Polymers such as polyether-*block*-polyamide (PEBAX) [17], polyimide [18], polyamide [19], polysulfone [20], poly(methyl methacrylate) (PMMA) [21], and poly(ethyl methacrylate) (PEMA) [22] have been used as selective layers.

 Springer

A thin film selective layer can be made via several methods including interfacial polymerization [23], solution coating [24], plasma polymerization [24, 25], casting [26], or other surface treatment methods [27]. One of the ways of surface treatment is surface-initiated atom transfer radical polymerization (ATRP) method [28–30]. ATRP is a method broadly applied for the decoration of different substrates by tethering polymer chains. This method has been widely examined for surface treatment in a flat geometry; however, it is less reported in the field of porous membranes [28]. Recently, surface-initiated polymerization to acquire polymer brush structure has received interest in gas separation [30], due to low polydispersity and well-controlled density of grafting on the selective polymer layer [28]. Balachandra and coworkers [30] synthesized cross-linked poly(ethylene glycol dimethacrylate) (PEGDMA) and poly(2-hydroxyethyl methacrylate) (PHEMA) on porous alumina by the ATRP method. The results showed that CO_2/CH_4 and O_2/N_2 selectivity of PEGDMA were ~20 and ~2, respectively. But PHEMA brushes showed only Knudsen diffusion-based selectivity. In another work, thin poly(ethylene oxide) (PEO)-based polymer films were grown from porous alumina substrates via ATRP. The membrane exhibited a CO_2/H_2 selectivity of 12 and a CO_2 permeability of about 20 barrers [31]. A poly(vinyl pyrrolidone) (PVP)-grafted poly(vinyl chloride) (PVC) copolymer was synthesized by ATRP. PVP grafting enhanced CO_2 permeability of PVC membrane up to 4-fold [32].

PVDF is extensively applied as membrane, owing to its excellent processability, chemical stability, and good thermal property [33–35]. However, PVDF has been recognized as a gas barrier material and its application in gas separation membranes is restricted by pores of the surfaces [34, 36]. It has been reported that sorption and permeation characteristics of porous membranes may be varied by surface covering with the polymeric layer [36]. Surface treatment could provide favorite modifications into the PVDF membranes, along with intact bulk properties [35]. Zhou and coworkers [11] developed PVDF-PDMS composite microfiltration membrane for separation of dimethyl carbonate (DMC) from a methanol solution. In another work, Chung and coworkers [12] fabricated a polysulfone-poly(dimethylsiloxane)-poly(4-vinylpyridine) (PSf-PDMS-PVP) multilayer composite hollow fiber membrane for gas separation. Composite hollow fiber membrane showed H_2/N_2, CO_2/CH_4, and O_2/N_2 selectivities of 100, 50, and 7, respectively. PDMS-porous polymer bilayer was investigated as gas separation and pervaporation membranes. For example, Prajapati and coworkers used PSf hollow fibers with different pore asymmetries as supports. Uniform PDMS layer over the porous PSf support exhibited excellent gas permeability and O_2/N_2 selectivity [37]. In another study, different composite membranes consisting of a polyethersulfone phase inversion membrane as a sublayer and a PDMS coating as a top layer have been prepared and characterized for pervaporation and gas separation applications [9, 38]. The effects of preparation parameters on the performance and morphology of PDMS/PSf membranes were investigated [39]. Scofield and coworkers prepared diblock copolymers (BCPs) consisting of poly(ethylene glycol) (PEG) and PDMS. BCPs were synthesized and blended with a commercially available PEBAX to form the active layer of TFC membranes via spin coating. TFC membranes containing PEG and PDMS BCPs increased up to 250% of the permeance of pure PEBAX composite membranes, while maintaining a CO_2/N_2 selectivity of 21 [40]. In another work, the PDMS/ceramic composite pervaporation membranes were fabricated and used in alcohol recovery, desulfuration, and solvent dehydration and coupled processes, in which the composite membranes exhibited high pervaporation performance and especially high permeate flux [41].

In another research [21], solution-casted PMMA resulted in a selectivity of 20 for CO_2/CH_4. Also, PMMA derivatives like PEMA exhibited a selectivity of 20 and a permeability of 7 barrers for CO_2/CH_4 and CO_2, respectively. PDMS is a desirable coating material in gas separation membrane owing to its high permeability [35, 36, 42, 43]. On the other hand, PVDF is a highly nonreactive thermoplastic with good mechanical and thermal properties and excellent chemical resistance [44]. In this work, PVDF was chosen as the support layer of the membrane, owing to its excellent properties. Despite the intrinsically low permeability of semicrystalline PVDF, the microporous structure of PVDF support layer undesirably increases its permeability. Therefore, the necessity of a second layer (coating layer) for controlled permeability was felt. PDMS coating layer penetrates defects into the selective layer and decreases the possibility of gas leakage through the defects, and the high permeability of PDMS makes it as the best candidate for coating layer. The bilayer membrane combined the advantages of PVDF and PDMS together. To achieve high selectivity, glassy polymers such as PMMA and PHEMA were chosen as the selective layer on the membrane. Surface initiated (SI)-ATRP was applied for grafting a thin film of PMMA and PHEMA on the PVDF-PDMS substrates, and the CO_2/N_2 selectivities of PHEMA- and PMMA-grafted membranes were examined and compared with the solvent-extracted PVDF-PDMS bilayer. The existence of a thin selective layer over a support providing sufficient mechanical stability guarantees high membrane permeability.

Experimental

Membrane fabrication

The fabrication steps of PHEMA-anchored PVDF-PDMS TFC membrane are outlined in Fig. 1. PDMS was coated on the PVDF support via a dip coating method using a PDMS/n-hexane (=20/80 v/v) solution to block the defects of the
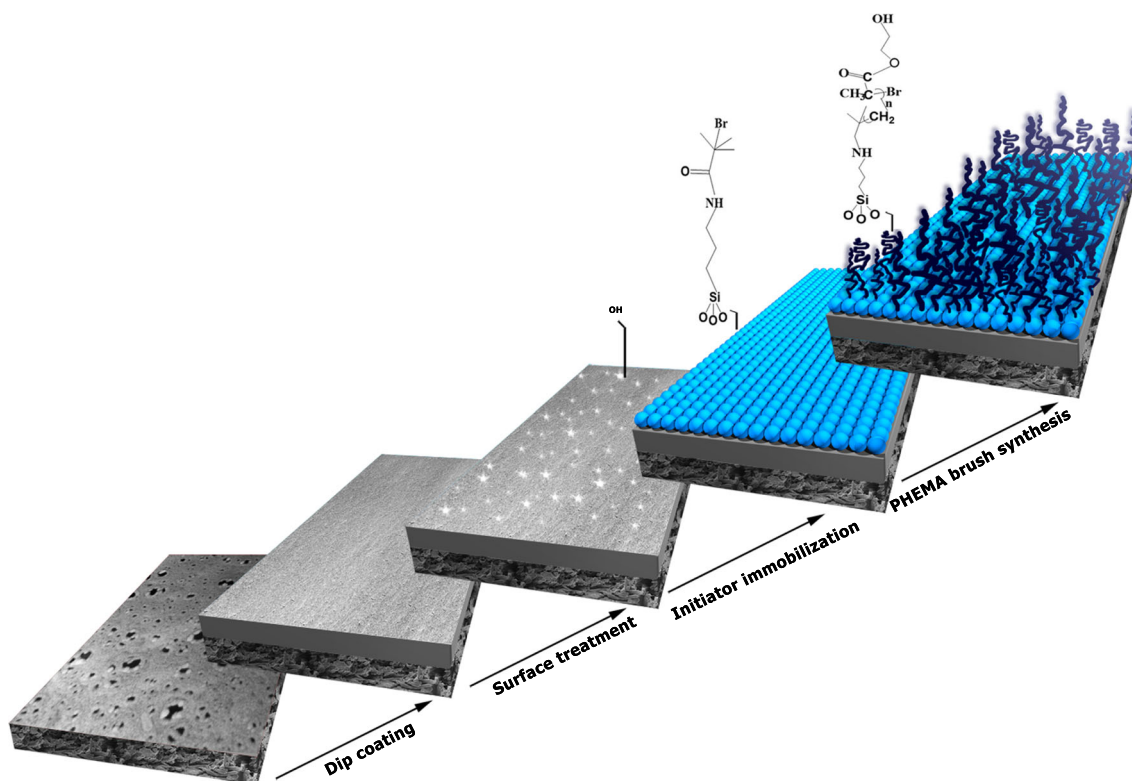
Fig. 1 Schematic illustrating the principle of preparing PHEMA-anchored PVDF-PDMS TFC membrane

selective layer thereby decreasing gas leakage possibility. Then, the membrane was dried at 70 °C in order to evaporate the residual solvent and partially cross-link the PDMS. After four times of dip coating of the mentioned PDMS/*n*-hexane solution on PVDF support, the coated support was maintained at 100 °C for 3 h to accomplish cross-linking. The samples were stored in a dry and dust-free environment. In the next step, PHEMA and PMMA were grafted on PVDF-PDMS substrate by ATRP. The water/methanol soluble monomers, methyl methacrylate (MMA), and 2-hydroxyethyl methacrylate (HEMA) were chosen to create a selective layer on the membranes. This was because, in addition to obtaining high selectivity, swelling of the PDMS in organic solvents (toluene, dichloromethane, etc.) [45] and destruction of substrate could be prohibited.

The PVDF-PDMS bilayer was treated by ultraviolet-ozone (UVO) radiation when it was submerged in water; then the initiator, 3-(2-bromoisobutyramido)propyl(trimethoxy) silane (BrTMOS), was immobilized on it, and finally, the monomers were polymerized by SI-ATRP.

Pretreatment of the substrates and initiator immobilization

The PVDF-PDMS bilayer was treated by UVO radiation for 2 h when it was submerged in water. The water medium was used to prevent wrinkling and cracking creation on PVDF-PDMS substrate due to UVO radiation [46]. The treated PDMS-PVDF membrane was laid in a mixture of ethanol (20 mL) and BrTMOS (0.5 g), which was synthesized according to Section B, Supplementary information, for 20 h at 30 °C in a N_2 environment. Then, the initiator-functionalized PVDF-PDMS TFC membrane was sonicated in water for 5 min. The initiator-functionalized membrane was then Soxhlet extracted in ethanol for 18 h and dried for 1 h at 70 °C.

Surface-initiated ATRP of HEMA (or MMA) on PVDF-PDMS substrate

High purity water (15 mL), methanol (15 mL), and HEMA (17.1 g, 130 mmol) (or MMA (13.0 g, 130 mmol)) were mixed in a 50-mL two-neck flask with a stirring bar, and four freeze-pump-thaw cycles were used for degassing. The solution was transferred into a round bottom flask containing the mixture of $CuBr_2$ (24.3 mg, 109.2 μmol), CuCl (111 mg, 1.13 mmol), and 2′,2-bipyridine (bipy) (435 mg, 2.79 mmol). The resulting mixture was transferred in the reaction flask continuously being purged with nitrogen including the initiator immobilized on the PVDF-PDMS substrate. The reaction was done for 24 h at 30 °C. Afterward, the polymer-tethered substrate was sonicated for 5 min in water and dried by a nitrogen flux. Then, PHEMA (or PMMA)-tethered PVDF-PDMS TFC was Soxhlet extracted for 18 h with methanol [47].

Characterization methods

The surface and cross section of the various dried substrates were sputtercoated with gold and viewed by a field emission scanning electron microscope (FESEM) (Tescan, MIRA3 FEG-SEM, Czech Republic). The cross sections were obtained by freeze-fractured membranes in liquid nitrogen. Water contact angles were measured by a contact angle measurement equipment (Sahand University of Technology, Tabriz, Iran) equipped with a DV-3000 binocular (Bell, Italy). Fourier transform infrared spectroscopy (FTIR) analysis was performed on a Tensor 27 spectrometer (Bruker, Germany) using an attenuated total reflection (ATR) unit. Atomic force microscopy was performed on a Dual Scope Probe Detector (DS 95-50-E, DME, Denmark) in tapping mode. Proton magnetic resonance spectra (^{1}H NMR) were registered on a Bruker DPX300 spectrometer operating at 300 MHz in deuterated chloroform (CDCl$_3$). X-ray photoelectron spectroscopy (XPS) data was documented with a 8025-BesTec twin anode XR3E2 X-ray source system. ESP300 Motion Controller/Driver ellipsometer equipped with Si/SiO$_2$ substrate and a He/Ne laser having the wavelength of 632.8 nm was applied to do ellipsometric measurements.

The molecular weight of PHEMA- or PMMA-cleaved polymer on Si wafer was determined by gel-permeation chromatography (GPC) using the Agilent 1100 HPLC system (Agilent Technologies, Palo Alto, CA, USA). The eluent was THF solvent at a flow rate of 1.0 mL/min. To cleave PMMA or PHEMA from the support, the PHEMA or PMMA-modified silicon wafer was placed in a Petri dish along with 2–3 mL of 10% solution of HF acid (49% reagent grade, Fisher). After 30 min, 10 mL of chloroform was added and stirred to capture the PHEMA or PMMA chains in the organic phase. The chloroform was extracted with a syringe and placed in a small vial (5 mL).

Gas permeation properties were determined by a circular disk permeation module with a pressure gauge. The permeate flux was recorded versus inlet pressure (2–5 bar) by a soap-bubble flow meter in order to check the carbon dioxide, nitrogen, and methane permeation. The bubble flow meter system is a simple and precise way to measure flow rates of gases. It determines the volumetric flow rate by measuring the time taken by the gas stream to move a soap bubble through a specific volume. For each gas, the permeation system was exposed to the flow of gas to obtain steady-state flux. In gas permeation analysis, three different membranes were tested for each sample. The membrane surface exposed to the gas was 19.6 cm^2. The overall selectivity of a membrane was calculated from the following relation [48]:

$$\alpha_{12} = \frac{P_1}{P_2} = \frac{S_1}{S_2} \cdot \frac{D_1}{D_2} \tag{1}$$

Where α_{12} and P are the selectivity and pure permeability for each gas, D_1/D_2 ratio is the mobility (or diffusivity) selectivity, and S_1/S_2 ratio is the solubility selectivity.

Results and discussion

Membrane characterization

The chemical composition of modified surfaces was characterized by ATR-FTIR analysis. The spectra of the neat PVDF-PDMS and PHEMA- and PMMA-anchored PVDF-PDMS TFC membranes are presented in Fig. 2. The absorption band that appeared at 1728 cm^{-1} was referred to the O–C=O stretching vibration of ester groups, which signified grafting of the PMMA and PHEMA onto the PVDF-PDMS substrates. The peak corresponding to the –OH groups in the spectral region 3300–3500 cm^{-1} (Fig. 2b) indicated that PHEMA was successfully anchored on PVDF-PDMS TFC membrane. After reaction of the film with the MMA monomer, there was a slight enhancement in the peak intensity in the spectral region 2945 cm^{-1} (Fig. 2c), which could be ascribed to C–H stretching vibration of the CH$_2$ group of the tethered PMMA.

The morphologies of the cross section and top surface for the pristine, PHEMA-anchored, and PMMA-anchored PVDF-PDMS TFC membranes were studied by FESEM. The image obtained from the cross section of the commercial PVDF membrane (Fig. 3a, left) revealed that the substrate consisted of two different layers. The SEM image of the top view of the commercial PVDF membrane revealed its porous structure (Fig. 3a, right). The top view SEM image of PVDF-PDMS (Fig. 3b, right) showed that coating of PDMS on the PVDF support caused coverage of pores on the PVDF membrane surface. The thickness of the PDMS layer was about 50 μ (Fig. 3b, left). As depicted, tethering of PHEMA (Fig. 3c) and PMMA (Fig. 3d) chains on PVDF-PDMS TFC caused a significant alteration in the morphology of the top surface of the membrane.

In addition to the analyses carried out on the brush-tethered membranes, to precisely validate the brush characteristics, we analyzed the brushes synthesized on silicon wafer. For this purpose, tapping mode AFM images (Fig. 4) were taken from the stepped samples of PHEMA brushes synthesized on silicon wafer. From the AFM results, the thickness of PHEMA brush was about 15 nm (Fig. 4). Contrary to the flat surfaces such as silicon and gold wafers which are more convenient reference substrates to characterize [49–52], because of high surface roughness of PVDF-PDMS, ellipsometry of its surface was impossible. Therefore, it was tried to use data of Si wafer to evaluate the properties of tethered chains (thickness, grafting density, etc.) on PVDF-PDMS bilayer. The thicknesses measured by ellipsometry were about 16 and 22 nm for PHEMA- and PMMA-anchored brushes, respectively, grown after 4 h. The thicknesses of PHEMA and PMMA brushes grown after polymerization for 24 h, measured by ellipsometry, were 47 and 54 nm, respectively.

The AFM images of the commercial PVDF, unmodified, initiator-immobilized, and PHEMA-anchored PVDF-PDMS

Fig. 2 ATR-FTIR spectra (normalized to the Si–O–Si peak at 1100 cm^{-1}) of the pristine (**a**), PHEMA-anchored (**b**), and PMMA-anchored (**c**) PVDF-PDMS substrates
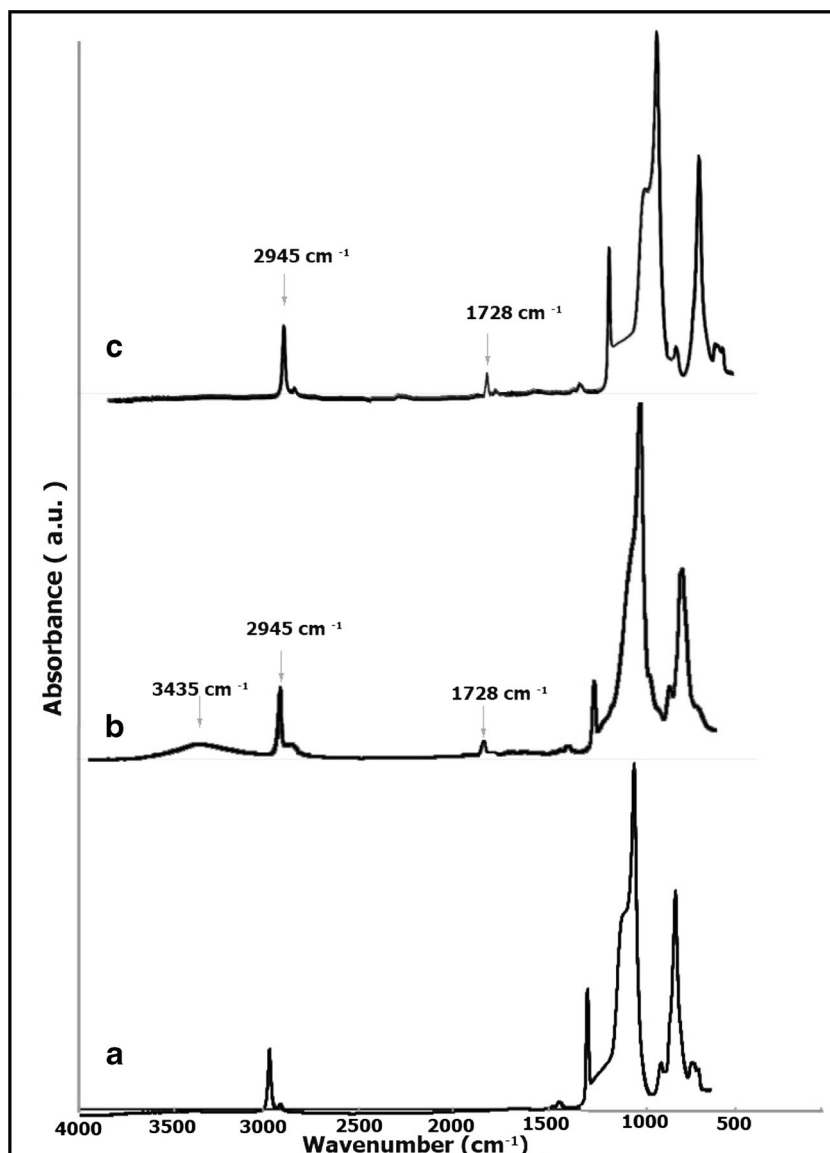

TFC membranes are shown in Fig. 5. These results revealed the change in surface morphology of PVDF support after PDMS coating. Comparing the AFM images showed that the PDMS-modified support (Fig. 5b) was smoother than the unmodified PVDF support (Fig. 5a), and the root mean square roughness (R_{rms}) was decreased from 75 to 9.9 nm. The value of R_{rms} was increased from 9.9 nm for the PDMS-covered PVDF to 16 nm for the initiator-immobilized substrate and 22.7 and 32.4 nm for the PHEMA- and PMMA-anchored PVDF-PDMS substrates, respectively.

Water contact angle (WCA) measurement was used as a tool to monitor the success of surface modification of the PVDF-PDMS TFC membrane in each step. While the WCA for neat PVDF-PDMS was ~96°, the WCA measured for UVO-treated PVDF-PDMS membrane after submerging in water was ~45°. An increase in the water contact angle occurred with immobilizing initiator, owing to the hydrophobic

characteristic of the initiator-coated surface; WCA of ~87° was observed for the initiator-immobilized PVDF-PDMS substrate. As seen in Fig. 6, the WCA after reaction of HEMA and MMA monomers with the initiator-immobilized surface changed to ~60° and ~72°, respectively.

Successful immobilizing of the BrTMOS initiator and grafting of PHEMA and PMMA chains on PVDF-PDMS substrate were also investigated by XPS. The XPS wide scan spectra of the neat and initiator-immobilized PVDF-PDMS membrane are shown in panels a and b of Fig. 7, respectively. The XPS spectra for PVDF-PDMS had four signals Si2s, Si2p, O1s, and C1s; the bromosilane initiator-immobilized support exhibited six signals at about 532, 285, 400, 153, 100, and 70 eV associated with O1s, C1s, N1s, Si2s, Si2p, and Br1s core level signals (Fig. 7b). The high-resolution elemental scan of C1s obtained from the bromosilane initiator-immobilized support (Fig. 8b) confirmed the
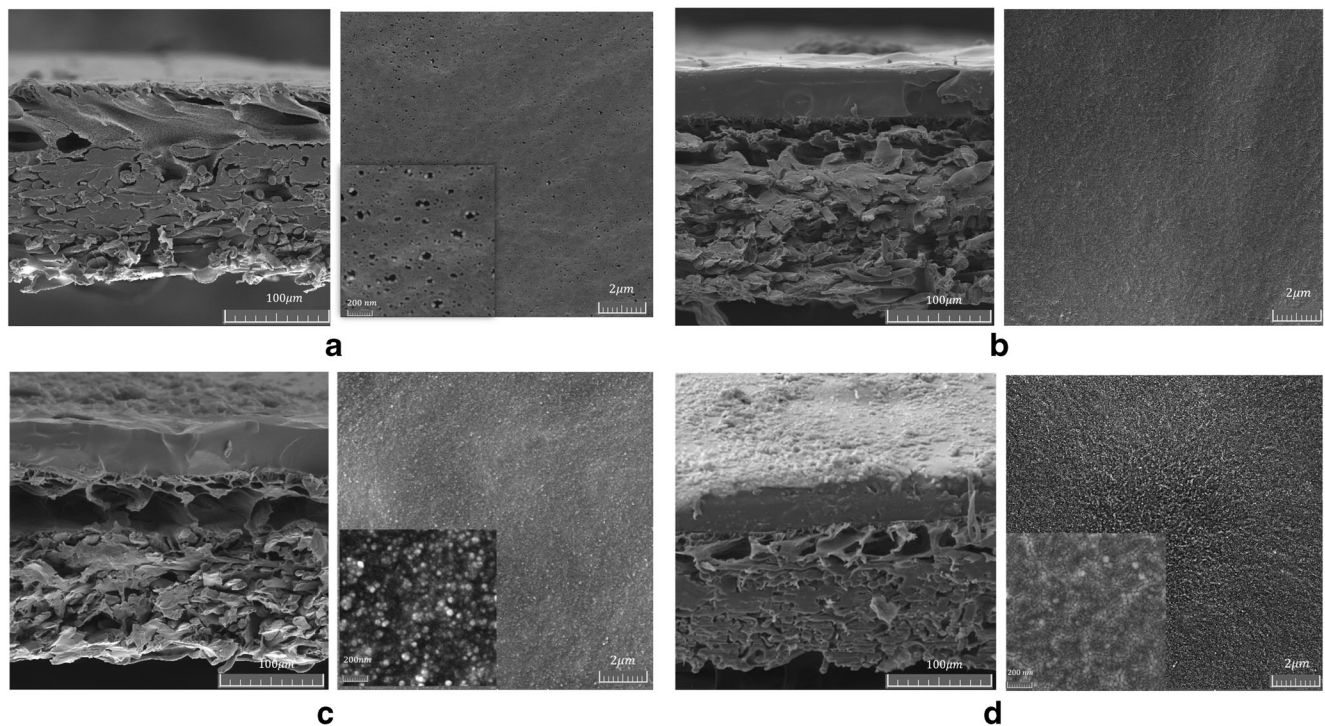
Fig. 3 FESEM images obtained from the cross section (*left images*) and top surface (*right images*) of **a** the commerical PVDF, **b** PDMS-coated PVDF, **c** PHEMA-anchored PVDF-PDMS, and **d** PMMA-anchored PVDF-PDMS TFC membranes. Polymerization time was 24 h

successful immobilization of initiator on PVDF-PDMS support. The C1s core level spectrum was legibly curve fitted with three components including binding energies (BEs) at about 284.0 eV (for C–C/C–H species), 286.9 eV (for C–O/C–Br species), and 289.7 eV (for N–C = O species).

The XPS results were also applied to detect grafting of PHEMA and PMMA brushes on PVDF-PDMS support. The XPS spectra for PHEMA- and PMMA-tethered PVDF-PDMS TFC membrane had four signals Si2s, Si2p, O1s, and C1s. The high-resolution elemental scan of C1s core level spectra were curve fitted with three components with BEs at about 284.3, 286.8, and 289.8 eV for PHEMA-tethered (Fig. 8c) and 285.1, 286.1, and 289.3 eV for

PMMA-tethered PVDF-PDMS (Fig. 8d), which were attributed to C–C/C–H, C–O/C–Br, and O–C=O species, respectively. The [C–H]:[C–O]:[O–C=O] molar ratios, as specified from the C1s spectral component area ratio, were 3.3:1.8:1 and 3.1:0.9:1 for PHEMA and PMMA brushes, respectively. These ratios deviated somewhat from the 3:2:1 theoretical ratio for PHEMA and 3:1:1 for PMMA that agree rather well with the corresponding theoretical values. Furthermore, comparisons of XPS spectra before and after grafting of PHEMA and PMMA confirmed the disappearance of the nitrogen peak, and Si2s and Si2p signals were decreased due to formation of brushes on the surface. The surface chemical composition obtained from XPS analysis

Fig. 4 AFM images (*left*) and 3D surface image (*right*) of the brush formed on a stepped silicon wafer after 4 h of polymerization
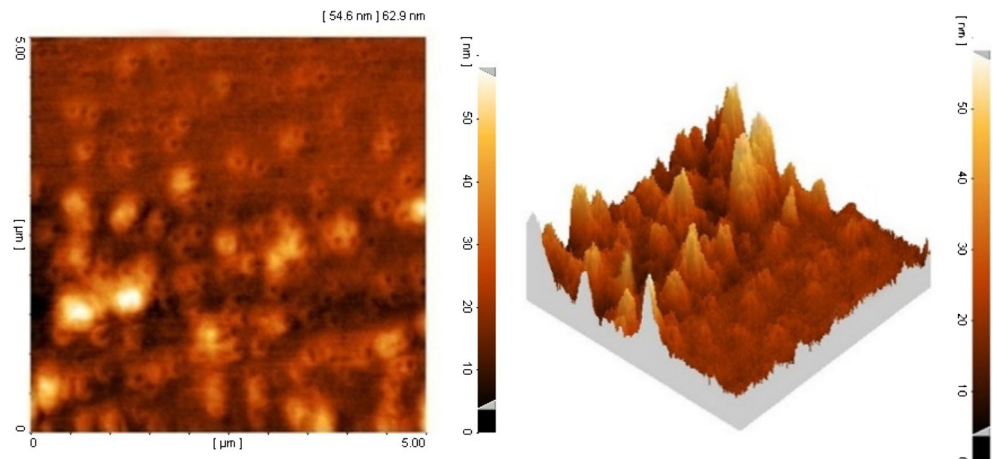
Fig. 5 AFM phase images and 3D surface images (*insets*) of the commercial PVDF (**a**), unmodified (**b**), initiator-immobilized (**c**), and PHEMA-anchored (**d**) PVDF-PDMS TFC membranes. The polymerization time was 24 h
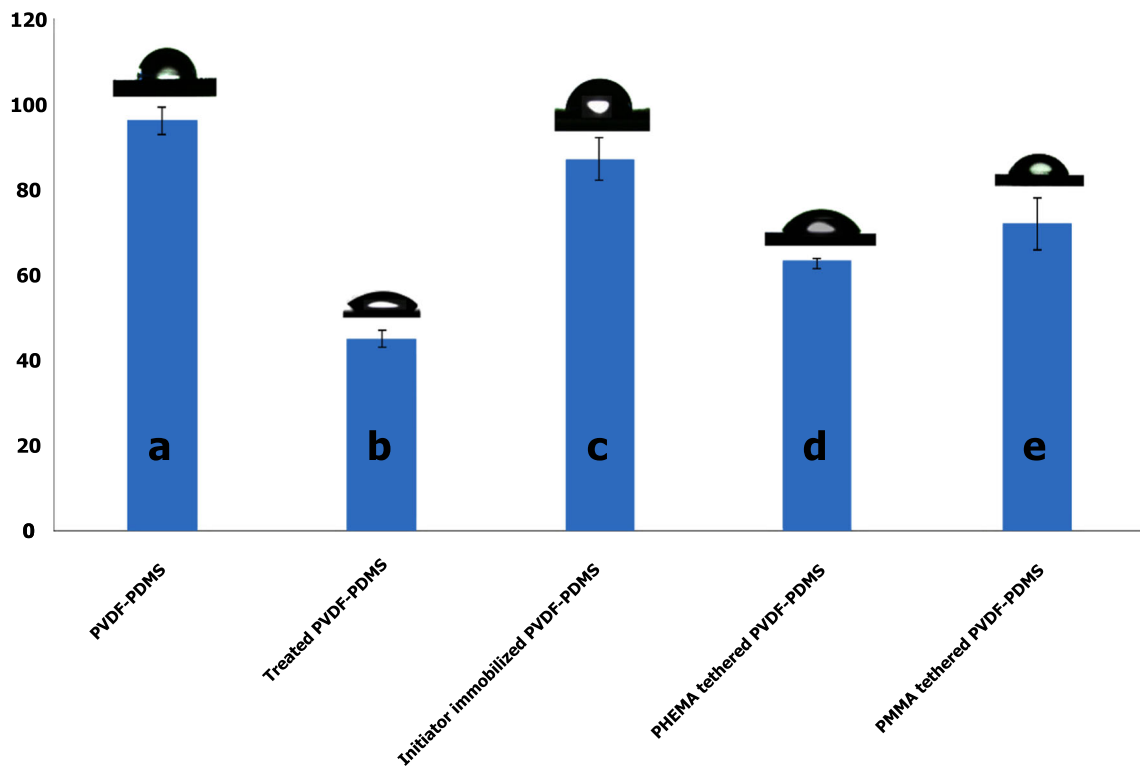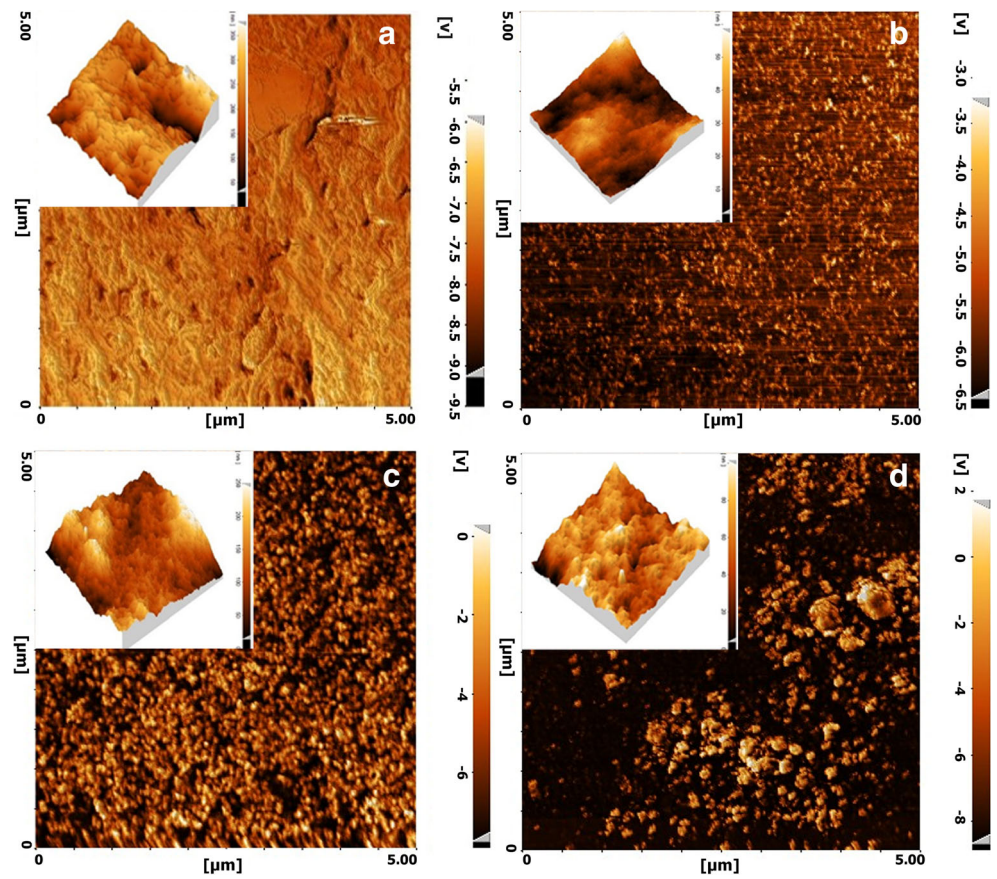
Fig. 6 WCA results of *a* the neat, *b* UVO-treated, *c* initiator-immobilized, *d* PHEMA-anchored, and *e* PMMA-anchored PVDF-PDMS TFC membranes
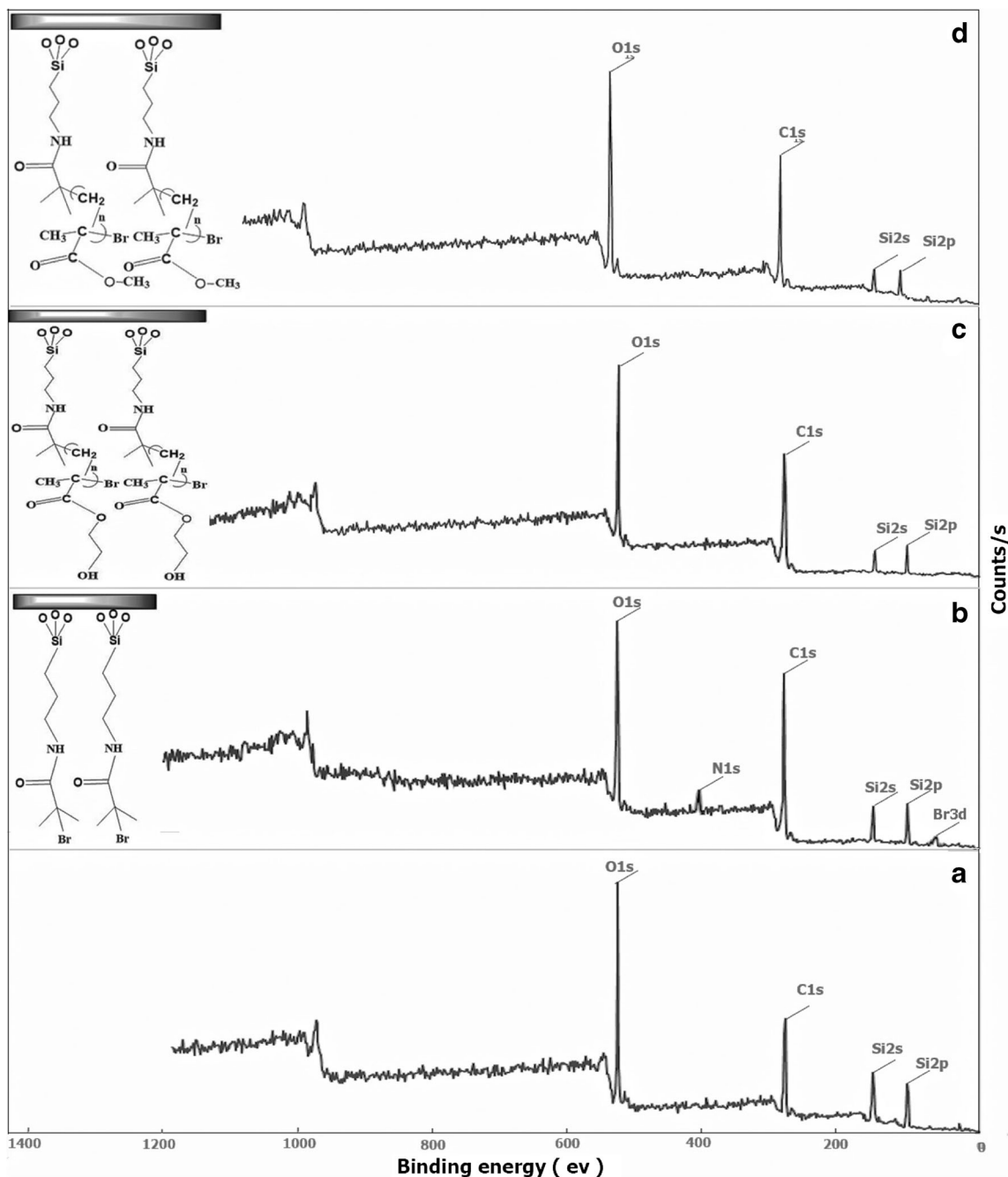
Fig. 7 XPS survey spectra of the neat (**a**), initiator-immobilized (**b**), PHEMA-anchored (**c**) and PMMA-anchored (**d**) PVDF-PDMS TFC membranes

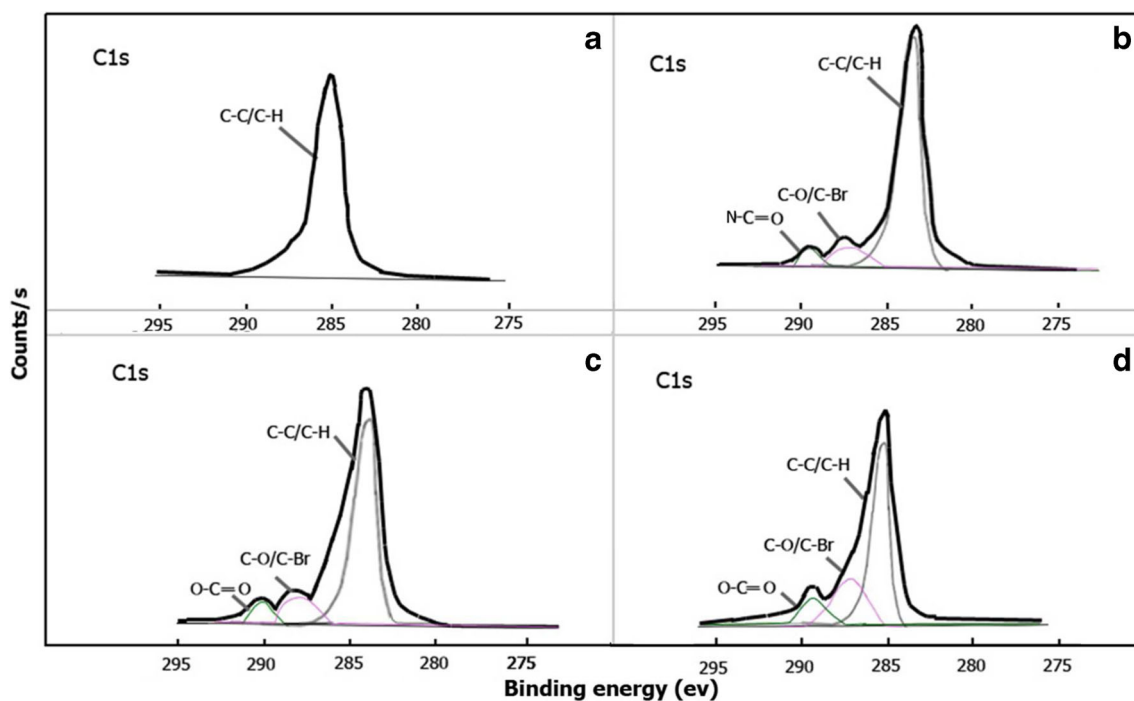of PVDF-PDMS (a), initiator-immobilized (b), PHEMA-grafted (c), and PMMA-grafted (d) PVDF-PDMS TFC membranes is reported in Table S2.

To control the grafting density of polymer brushes prepared by SI-ATRP, one of the basic requirements is the control of the chemical composition and graft density of the immobilized ATRP initiator. As mentioned in the Supporting information (Section C), the initiator grafting density on Si wafer and PVDF-PDMS bilayer was determined by the modified Cassie-Baxter equation [53] (Eqs. (S1) and (S2)). The initiator

grafting density was about 3 and 3.4 no./nm^2 for the Si wafer and PVDF-PDMS bilayer, respectively. This data was confirmed by the Br/Si ratio (0.0031) estimated from XPS results for the initiator-immobilized PVDF-PDMS membrane (Table S2). After grafting of PHEMA and PMMA on Si wafer, the results of grafting density (Σ) and distance between grafting sites (S) of cleaved PHEMA and PMMA on Si wafer were calculated by Eqs. (S4) and (S5). The results of grafting densities 0.67 and 0.63 were calculated for cleaved PHEMA and PMMA on Si wafer, respectively (Table 1). Reduced

Fig. 8 High-resolution elemental scans of C1s signals of PVDF-PDMS (a), initiator-immobilized (b), PHEMA-grafted (c), and PMMA-grafted (d) PVDF-PDMS TFC membranes

grafting density after grafting of polymers confirmed that alkoxysilanes (initiator) are suspicious of being hydrolyzed in aqueous media [54].

Gas permeability

Although PVDF membranes have very low permeability due to the intrinsically low permeability of semicrystalline PVDF [55], as shown in Fig. 3a, the commercial PVDF exhibited some large pores with sizes larger than 0.1 μm. Hence, it did not have resistance against gas permeability, which limits PVDF application in gas separation. Supported membranes were prepared on porous PVDF by dip coating in PDMS solution in *n*-hexane. With this procedure, a nanoporous PDMS layer with a thickness of less than 50 μm was obtained. High permeability and low selectivity are the general features of rubbery polymers, in contrast to glassy polymers. Differences in gas solubility are the basis of gas separation by rubbery polymer membranes, whereas gas diffusivity is the determinant factor in the glassy polymer membranes [56].

Figure S3 indicates that the multilayer PDMS-coated PVDF porous membrane facilitated the transport and improved the performance for gas separation. The CO_2

permeance of PVDF-PDMS was 8.5×10^{-8} mol/(m^2 s Pa) at 3 atm (Table 2).

From Table S3, the solubility coefficient in PDMS polymer affected the permeability value much more than the diffusion coefficient. The more the difference in the relative size of two penetrating gases, the more the diffusion selectivity. However, the solubility selectivity increases with an enhancement in the condensability difference. Therefore, solubility, diffusivity, and overall selectivity are mainly affected by the relative value of the two pointed terms.

Based on the size of the permeating gas, the permeability coefficient for the smaller size gases is expected to have high value compared to larger size more condensable gases [57]. However, the condensable gases were observed to have very high permeability values in PDMS. Increasing the penetrant concentration with time enhanced the polymer matrix plasticization, especially in the case of adsorbing penetrants. In a plasticized polymer, the penetrant diffusivity increases, which is resulted by enhanced local segmental mobility of the polymer matrix. On the contrary, a significant penetrant pressure, owing to its high concentration, leads to polymer compression to some extent and consequent decreasing of penetrant diffusion coefficients. Therefore, penetrants with lower adsorption

Table 1 Molecular weight, PDI, and grafting density were calculated for cleaved PHEMA and PMMA on Si wafer

Polymer brushes	Thickness (nm)	ρ (g/cm³)	M_n/1000 (g/mol)	M_w/M_n	Σ (chains/nm²)	S (nm)
PHEMA	47	1.15	48.56	1.3	0.67	1.38
PMMA	54	1.19	61.40	1.5	0.63	1.42

Table 2 Gas permeance (permeability/thickness) coefficients estimated for pristine PVDF-PDMS, PVDF-PDMS after solvent extraction, and PHEMA- and PMMA-grafted PVDF-PDMS TFC membranes

Sample	Pressure (bar)											
	2			3			4			5		
	Calculated gas permeance coefficients ×10^8 (mol/(m^2 s Pa))											
	CO$_2$	N$_2$	CH$_4$	CO$_2$	N$_2$	CH$_4$	CO$_2$	N$_2$	CH$_4$	CO$_2$	N$_2$	CH$_4$
PVDF-PDMS	8.3 ± 0.8	0.9 ± 0.2	2.1 ± 0.2	8.5 ± 1.0	1.0 ± 0.3	2.1 ± 0.5	8.6 ± 0.6	1.0 ± 0.1	2.5 ± 0.1	8.9 ± 0.8	0.1 ± 0.0	2.3 ± 0.3
PVDF-PDMS[a]	8.9 ± 0.6	1.7 ± 0.5	6.4 ± 0.8	8.7 ± 0.4	1.4 ± 0.3	5.5 ± 0.4	9.2 ± 0.8	1.4 ± 0.0	5.5 ± 0.3	9.2 ± 0.8	1.6 ± 0.5	5.8 ± 0.3
PVDF-PDMS-PHEMA	1.2 ± 0.3	0.1 ± 0.0	0.3 ± 0.0	1.2 ± 0.1	0.1 ± 0.0	0.3 ± 0.0	1.2 ± 0.2	0.1 ± 0.0	0.3 ± 0.0	1.2 ± 0.3	0.1 ± 0.0	0.2 ± 0.2
PVDF-PDMS-PMMA	1.5 ± 0.3	0.1 ± 0.0	0.21 ± 0.3	1.8 ± 0.4	0.1 ± 0.0	0.3 ± 0.1	2.5 ± 0.1	0.1 ± 0.0	0.4 ± 0.0	2.6 ± 0.4	0.1 ± 0.0	0.4 ± 0.1

The reported values are the average of permeance coefficients for three different membranes

[a] PVDF-PDMS after solvent extraction

like nitrogen have low permeability value compared to the more soluble penetrants (CO_2) which induce significant plasticization. From the results, one can observe that difference in penetrate solubility is a substantial factor in the determination of rubbery polymer selectivity [57].

To synthesize the polymer brush with SI-ATRP, the membranes were placed in the ATRP solution. In contrast to water, nonpolar solvents (e.g., hydrocarbons, toluene, and dichloromethane) are capable of PDMS swelling [45]. The swelling significantly reduces the adhesion between PDMS coating and PVDF substrate, which affects the membrane performance. Fortunately, PDMS has a slight swelling in methanolic and ethanolic solutions [29]. Therefore, in this work, the aqueous solution of methanol was employed as a reaction medium for ATRP.

On the other hand, the high dielectric constant of the polar solvents such as water likely improves the catalyst activity [29]. So, this method quickly increases the rate of polymerization to grow brushes (of water-soluble monomers). This strategy allows the formation of brushes with a predetermined length. Before performing ATRP, the membranes were extracted in methanol and ethanol separately. As shown in Tables 2 and 3, the permeance increased and selectivity of the membranes decreased in methanol and ethanol extraction. For example, the CO_2/N_2 selectivity of PVDF-PDMS decreased from about 9 to 6, and also, the CO_2/CH_4 selectivity of PVDF-PDMS at 3 atm decreased from about 4 to 1.6 after solvent extraction. It has previously been demonstrated that the curing process of PDMS relies on time and temperature and does not reach complete cross-linking, and about 5 wt% of PDMS mass remains uncross-linked, which can be extracted by solvents [58, 59]. These low molecular weight oligomers can diffuse freely and change the surface characteristics of the elastomer [60–62]. The amount of extractable components of the PDMS used in this work was about 3.3 wt%. In comparison to the virgin PVDF-PDMS membrane, the extracted one exhibited better stability and was selected as reference sample for permeability studies.

After preparation of the two-layer membrane, PVDF as the support and PDMS as the coating layer, PHEMA and PMMA chains were synthesized onto the membrane as selective layers. This composite membrane including a thin selective layer (PHEMA or PMMA brushes) and a porous support (PVDF) is desirable in gas separation due to high gas flow.

Table 3 shows the fluxes of carbon dioxide, nitrogen, and methane gases through a PVDF-PDMS, solvent-extracted PVDF-PDMS, and PHEMA- and PMMA-anchored PVDF-PDMS TFC membranes versus transmembrane pressure. After grafting of PHEMA and PMMA, the permeance coefficient of different gases decreased as $CH_4 > CO_2 > N_2$. Glassy polymers such as PHEMA and PMMA have low permeability as compared to rubbery ones. They have rigid chains that may retard the penetration of gas molecules between

Table 3 Ideal selectivities for pristine PVDF-PDMS, PVDF-PDMS after solvent extraction, and PHEMA- and PMMA-grafted PVDF-PDMS TFC membranes

Sample	Pressure (bar)							
	2		3		4		5	
	Calculated gas selectivity coefficients							
	CO_2/N_2	CO_2/CH_4	CO_2/N_2	CO_2/CH_4	CO_2/N_2	CO_2/CH_4	CO_2/N_2	CO_2/CH_4
PVDF-PDMS	9.5 ± 0.4	4.0 ± 0.2	8.9 ± 0.4	4.0 ± 0.8	8.8 ± 0.5	3.6 ± 0.3	7.8 ± 0.8	3.8 ± 0.4
PVDF-PDMS[a]	5.4 ± 0.2	1.4 ± 0.7	6.2 ± 0.3	1.6 ± 0.3	6.4 ± 0.5	1.6 ± 0.4	5.8 ± 0.3	1.6 ± 0.2
PVDF-PDMS-PHEMA	14.0 ± 1.2	3.8 ± 0.3	14.2 ± 1.8	4.3 ± 0.4	15.3 ± 1.6	4.4 ± 0.5	15.5 ± 2	5.5 ± 0.9
PVDF-PDMS-PMMA	20.0 ± 2.4	7.1 ± 0.4	19.3 ± 1.3	7.0 ± 0.7	19.1 ± 1.6	7.2 ± 0.5	19.3 ± 1.8	7.0 ± 0.8

[a] PVDF-PDMS after solvent extraction

intersegmental polymer chains [63]. Therefore, grafting of PHEMA or PMMA brushes onto PVDF-PDMS as a third layer was expected to reduce the permeance of PHEMA- and PMMA-grafted PVDF-PDMS membranes. The tighter packing of grafted chains limited the diffusion of all molecules, but it limited the diffusion of large molecules more than that of small molecules. Therefore, the materials became increasingly size selective. For instance, a linear molecule, CO_2 (kinetic diameter = 0.33 nm), diffused more quickly than spherical molecules of CH_4 (kinetic diameter = 0.38 nm) and N_2 (kinetic diameter = 0.36 nm) [30, 64].

Table 3 indicates that methanol and ethanol extraction decreased the selectivity of CO_2/N_2 and CO_2/CH_4 due to the mechanical instability caused by swelling in the solvents [45]. The solvents can dissolve the polymer if it is not cross-linked [59]. As shown, after ATRP, the CO_2/N_2 selectivity of PHEMA- and PMMA-anchored PVDF-PDMS TFC membranes increased to 14.7 and 19.4, respectively, but the CO_2/CH_4 selectivity of PHEMA- and PMMA-anchored PVDF-PDMS membranes was about 4.5 and 7, respectively. Balachandra and coworkers [30] used the SI-ATRP method to graft PHEMA on modified porous alumina. Despite the expectation, the observed CO_2/CH_4 and CO_2/N_2 selectivities for PHEMA were 0.7 and 0.9, respectively, and permeability coefficients for PHEMA were about 7 barrers. In this study, PVDF-PDMS-PHEMA trilayer increased permeability from 7 to 1680 barrers and CO_2/CH_4 and CO_2/N_2 selectivities increased to 4.5 and 14.7, respectively.

Compared to other gases, CO_2 permeation is considerable due to small diameter and high condensability [65]. In addition, polar CO_2 molecules can interact with the polar carbonyl groups existing in the PMMA and PHEMA structures and the hydroxyl groups in the PHEMA structure. The condensability of N_2 (71 K) was less than the condensability of CO_2 (195 K) and CH_4 (149 K) and N_2 had no special interaction with the PHEMA and PMMA brushes, and their selectivities are mediated by molecular sieve characteristic. Since the gas pairs of CO_2/N_2 and CO_2/CH_4 experienced high diffusivity selectivity,

high affinity of CO_2 with the carbonyl and OH groups on the PMMA and PMMA brushes enhanced the solubility selectivity of this gas. The high CO_2/N_2 selectivity with respect to CO_2/CH_4 selectivity was ascribed to very lower condensability of N_2 than that of CH_4. However, higher diffusivity selectivity for the CO_2/CH_4 pair is expected due to larger methane molecule; the governing role of solubility selectivity diminishes the total selectivity for CO_2/CH_4 [66].

Different selectivity of PHEMA- and PMMA-anchored PVDF-PDMS membranes was due to different functional groups in PHEMA and PMMA brushes; the carbonyl groups of PMMA and PHEMA brushes have greater ability to dissolve CO_2 than hydroxyl groups of PHEMA brushes [67]. Commonly, the more polar groups are added to the polymers, the more is the solubility parameter which in turn lowers the free volume and enhances chain stiffness, both decreasing CO_2 diffusivity [68, 69]. As mentioned, gas separation of glassy polymer membranes is caused mainly by differences in gas diffusivity [56]. The governing role of the difference in gas diffusivity in the separation mechanism makes one suppose that PHEMA brush has lower diffusion coefficient and overall selectivity than PMMA brush.

Conclusions

TFCs of PHEMA and PMMA chain-tethered PVDF-PDMS trilayers were prepared as a gas separation membrane. Atomic force microscopy was employed to monitor surface morphologies of membranes. The RMS roughness of the PVDF-PDMS bilayer (9.9 nm) increased to 22.7 and 32.4 nm for PVDF-PDMS-PHEMA and PVDF-PDMS-PMMA membranes, respectively. Water contact angle decreased from ~96° for neat PVDF-PDMS to ~45° for the treated PVDF-PDMS, respectively. After initiator immobilization on PVDF-PDMS bilayer, WCA increased to ~87°. WCA values for PHEMA- and PMMA-anchored PVDF-PDMS

membranes changed to ~60° and ~72°, respectively. The results of permeability measurements showed that after applying PDMS layer on PVDF substrate, it provided a suitable substrate for gas separation. After solvent extraction, the permeability of carbon dioxide, nitrogen, and methane gases of PVDF-PDMS substrate increased in all transmembrane pressures. After formation of a thin film consisting of PHEMA or PMMA, the CO_2/N_2 selectivity of PHEMA (=14.7) and PMMA (=19.4)-grafted PVDF-PDMS membranes increased by ~2- and ~3-folds, respectively, compared with solvent-extracted PVDF-PDMS (=6). Although the CO_2/CH_4 selectivity decreased from 3.5 to 1 after solvent-extraction of the PVDF-PDMS support, grafting PHEMA and PMMA on PDMS-coated PVDF substrate increased the CO_2/CH_4 selectivity to about 6 and 7, respectively.

Compliance with ethical standards

Conflict of interest The authors declare that they have no conflict of interest.

References

1. Chen HZ, Xiao YC, Chung TS (2011) Multi-layer composite hollow fiber membranes derived from poly(ethylene glycol) (PEG) containing hybrid materials for CO_2/N_2 separation J Membr Sci 381:211–220

2. Pinnau I, Wijmans JG, Blume I, Kuroda T, Peinemann KV (1988) Gas permeation through composite membranes J Membr Sci 37:81–88

3. Kattula M, Ponnuru K, Zhu L, Jia W, Lin H, Furlani EP (2015) Designing ultrathin film composite membranes: the impact of a gutter layer Sci Rep 5:15016

4. Liao S, Wang W, Uo M, Ohkawa S, Akasaka T, Tamura K, Cui F, Watari F (2005) A three-layered nano-carbonated hydroxyapatite/collagen/PLGA composite membrane for guided tissue regeneration Biomaterials 26:7564–7571

5. Henis JMS, Tripodi MK (1981) Composite hollow fiber membranes for gas separation: the resistance model approach J Membr Sci 8:233–246

6. Ulbricht M (2006) Advanced functional polymer membranes Polymer 47:2217–2262

7. Landrivon E, Miachon S, Kumakiri I, Matsukata M, Dalmon JA (2003) MFI-alumina composite membrane: influence of the support porous structure on the superlative performance Fuel Chem Div Prepr 48:394–395

8. Cybulski A, Moulijn JA, Stankiewicz A (2010) Novel concepts in catalysis and chemical reactors: improving the efficiency for the future. Wiley-VCH, Weinheim,

9. Shi E, Huang W, Xiao Z, Li D, Tang M (2007) Influence of binding interface between active and support layers in composite PDMS membranes on permeation performance J Appl Polym Sci 104:2468–2477

10. Mhlanga SD, Tshabalala TG, Nxumalo EN, Mamba BB (2014) Synthesis of PVDF ultrafiltration membranes supported on polyester fabrics for separation of organic matter from water IOP Conf Ser Mater Sci Eng 64:220–226

11. Zhou H, Lv L, Liu G, Jin W, Xing W (2014) PDMS/PVDF composite pervaporation membrane for the separation of dimethyl carbonate from a methanol solution J Membr Sci 471:47–55

12. Chung TS, Shieh JJ, Lau WWY, Srinivasan MP, Paul DR (1999) Fabrication of multi-layer composite hollow fiber membranes for gas separation J Membr Sci 152:211–225

13. Chung TS, Kafchiniski ER, Kohn RS, Foley P, Straff RS (1994) Fabrication of composite hollow fibers for air separation J Appl Polym Sci 53:701–708

14. Lundy KA, Cabasso I (1989) Analysis and construction of multi-layer composite membranes for the separation of gas mixtures Ind Eng Chem Res 28:742–756

15. Gleason KK (2015) CVD polymers: fabrication of organic surfaces and devices. Wiley-VCH, Weinheim

16. Rijn CJMV (2004) Nano and micro engineered membrane technology from the membrane. Science and technology series. Elsevier, Amsterdam

17. J.S. Louie, Fouling-resistant coatings for reverse osmosis membranes: gas and liquid permeation studies on morphology and mass transport effects, Ph.D. thesis, Stanford University, 2008.

18. Marek M, Brynda E, Pientka Z, Schauer J (1997) Crosslinked ultrathin polyimide film as a gas separation layer for composite membranes Eur Polym J 33:1717–1721

19. Dodda JM, Remis T, Tomas M, Novotny P (2016) Effect of alternation of polyamide selective layers in the formation and performance of thin-film composite membranes Desalin Water Treat 57:8720–8729

20. Ding C, Yin J, Deng B (2014) Effects of polysulfone (PSf) support layer on the performance of thin-film composite (TFC) membranes Chem Process Eng 1:1–8

21. Raymond PC, Paul DR (1990) Sorption and transport of pure gases in random styrene/methyl methacrylate copolymers J Polym Sci B Polym Phys 28:2079–2102

22. Chiou JS, Paul DR (1989) Gas sorption and permeation in poly(ethyl methacrylate) J Membr Sci 45:167–189

23. A. Sagle and B. Freeman, Fundamentals of membranes for water treatment, the future of desalination in Texas, 2004, 2, Report number 363, 137–154.

24. Baker RW (2004) Membrane technology and applications, 2nd edn. Wiley, New York

25. Yasuda HK (2005) Some important aspects of plasma polymerization Plasma Process Polym 2:293–304

26. Sapkal VS, Bansod PG, Sapkal RS (2011) Development of casting techniques for polyethersulfone ultra filtration membranes and their effects on flux and rejection Int J Chem Sci Appl 2:156–161

27. Saqib J, Aljundi IH (2016) Membrane fouling and modification using surface treatment and layer-by-layer assembly of polyelectrolytes: state-of-the-art review J Water Process Eng 11:68–87

28. Mittal V (2012) Polymer brushes: substrates, technologies, and properties. CRC, New York

29. Zeng F, Shen Y, Zhu S, Pelton R (2000) Atom transfer radical polymerization of 2-(dimethylamino) ethyl methacrylate in aqueous media J Polym Sci A Polym Chem 38:3821–3827

30. Balachandra AM, Baker GL, Bruening ML (2003) Preparation of composite membranes by atom transfer radical polymerization initiated from a porous support J Membr Sci 227:1–14

31. X. Dong, Reverse-selective gas separation membranes prepared by atom transfer radical polymerization, Ph.D. thesis, Michigan State University, 2012.

32. Yeon SH, Ahn SH, Kim JH, Lee KB, Jeong Y, Hong SU (2012) Synthesis and gas permeation properties of poly(vinyl chloride)-graft-poly(vinyl pyrrolidone) membranes Polym Adv Technol 23:516–521

33. Seiler DA (1997) PVDF in the chemical process industry. In: Scheirs J (ed) Modern fluoropolymers. Wiley, Chichester, pp. 487–505

34. Feijani EA, Tavasoli A, Mahdavi H (2015) Improving gas separation performance of poly(vinylidene fluoride) based mixed matrix membranes containing metal organic frameworks by chemical modification Ind Eng Chem Res 54:12124–12134

35. Ying L, Wang P, Kang ET, Neoh KG (2002) Synthesis and characterization of poly(acrylic acid)-graft-poly(vinylidene fluoride) co-polymers and pH-sensitive membranes Macromolecules 35:673–679

36. Chen Y, Deng Q, Xiao J, Nie H, Wu L, Zhou W, Huang B (2007) Controlled grafting from poly(vinylidene fluoride) microfiltration membranes via reverse atom transfer radical polymerization and antifouling properties Polymer 48:7604–7613

37. Prajapati PK, Kansara AM, Singh PS (2016) Preparation and characterization of an oxygen permselective polydimethylsiloxane hollow fibre membrane RSC Adv 6:88943–88953

38. Gudernatsch W, Menzel T, Strathmann H (1991) Influence of composite membrane structure on pervaporation J Membr Sci 61:19–30

39. Pakizeh M, Mansoori SAA, Pourafshari Chenar M, Namvar-Mahboub M (2013) Modification of PSf membrane nanostructure using different fabrication parameters and investigation of the CO_2 separation properties of PDMS-coated PSf composite membranes Braz J Chem Eng 30:345–354

40. Scofield JMP, Gurr PA, Kim J, Fu Q, Halim A, Kentish SE, Qiao GG (2015) High-performance thin film composite membranes with well-defined poly(dimethylsiloxane)-b-poly(ethylene glycol) co-polymer additives for CO_2 separation J Polym Sci A Polym Chem 53:1500–1511

41. Gongping L, Wang W, Wanqin J, Nanping X (2012) Polymer/ceramic composite membranes and their application in pervaporation process Chin J Chem Eng 20:62–70

42. Yampolskil Y (2010) Membrane gas separation. Wiley, Chichester

43. Reijerkerk SR, Knoef MH, Nijmeijer K, Wessling M (2010) Poly(ethylene glycol) and poly(dimethyl siloxane): combining their advantages into efficient CO_2 gas separation membranes J Membr Sci 352:126–135

44. Dong W, Wang H, Ren F, Zhang J, He M, Wu T, Li Y (2016) Dramatic improvement in toughness of PLLA/PVDF blends: the effect of compatibilizer architectures ACS Sustain Chem Eng 4(8):4480–4489

45. Rumens CV, Ziai MA, Belsey KE, Batchelor JC, Holder SJ (2015) Swelling of PDMS networks in solvent vapours; applications for passive RFID wireless sensors J Mater Chem C 3:10091–10098

46. Maher BM, Rezaali J, Jalili K, Abbasi F (2016) Effects of various treatments on silicone rubber surface, rubber chemistry and technology. doi:10.5254/rct.16.83782

47. Emmenegger CR, Avramenko OA, Brynda E, Skvor J, Alles AB (2011) Poly(HEMA) brushes emerging as a new platform for direct detection of food pathogen in milk samples Biosens Bioelectron 26:4545–4551

48. Peter J, Peinemann KV (2009) Multilayer composite membranes for gas separation based on crosslinked PTMSP gutter layer and partially crosslinked Matrimid 5218 selective layer J Membr Sci 340:62–72

49. Sui X, Zapotoczny S, Benetti EM, Schön P, Vancso GJ (2010) Characterization and molecular engineering of surface-grafted polymer brushes across the length scales by atomic force microscopy J Mater Chem 20:4981–4993

50. Sun K, Yang W, Ma G, Wan F, Gao J, Lei Z, Guo H (2011) Preparation of tunable wettability polymer (ionic liquid) brushes at rough substrate using surface initiated atom transfer radical polymerization J Braz Chem Soc 22:478–483

51. S. Hansson, ARGET ATRP as a tool for cellulose modification, Ph.D. thesis, Kungliga Tekniska högskolan, Stockholm 2012.

52. Yang Y, Bittner AM, Baldelli S, Kern K (2008) Study of self-assembled triethoxysilane thin films made by casting neat reagents in ambient atmosphere Thin Solid Films 516:3948–3956

53. Lego B, Francois M, Skene WG, Giasson S (2009) Polymer brush covalently attached to OH-functionalized mica surface via surface-initiated ATRP: control of grafting density and polymer chain length Langmuir 25:5313–5321

54. Arkles B, Steinmetz JR, Zazycny J, Mehta P (1992) Factors contributing to the stability of alkoxysilanes in aqueous solution. In: Mittal KL (ed) Silanes and other coupling agents. VSP, Utrecht, pp. 91–104

55. Choi SH, Tasselli F, Jansen JC, Barbieri G, Drioli E (2010) Eur Polym J 46:1713–1725

56. Mark JE (2006) Physical properties of polymers handbook, 2nd edn. Springer, New York

57. Reddy BSR, Senthilkumar U (2003) Prospects of siloxane membrane technology for gas separation—a review J Sci Ind Res 62:666–677

58. Lee J, Park C, Whitesides G (2003) Solvent compatibility of PDMS-based microfluidic devices Anal Chem 75:6544–6554

59. Regehr KJ, Domenech M, Koepsel JT, Carver KC, Zelski SJE, Murphy WL, Schuler LA, Alarid ET, Beebe DJ (2009) Biological implications of polydimethylsiloxane-based microfluidic cell culture Lab Chip 9:2132–2139

60. Kim J, Chaudhury M, Owen MJ (2000) Hydrophobic recovery of polydimethylsiloxane J Colloid Interface Sci 226:231–236

61. Eddington D, Puccinelli J, Beebe D (2006) Sensors Actuators 114:170–172

62. Bodas D, Malek CK (2007) Hydrophilization and hydrophobic recovery of PDMS by oxygen plasma and chemical treatment- an SEM investigation Sensors Actuators B Chem 123:368–373

63. Li NN, Fane AG, Ho WSW, Matsuura T (2008) Advanced membrane technology and applications. Wiley, New Jersey

64. Ghosal K, Freeman BD (1994) Gas separation using polymer membranes: an overview Polym Adv Technol 5:673–697

65. Yampolskii YP, Pinnau I, Freeman BD (2006) Materials Science of membranes for gas and vapor separation. Wiley, Chichester

66. Ameri E, Sadeghi M, Zarei N, Pournaghshband A (2015) Enhancement of the gas separation properties of polyurethane membranes by alumina nanoparticles J Membr Sci 479:11–19

67. Gui X, Tang Z, Fei W (2011) Solubility of CO_2 in alcohols, glycols, ethers, and ketones at high pressures from (288.15 to 318.15) K J Chem Eng Data 56:2420–2429

68. Sperling LH (1992) Introduction to physical polymer science. Wiley, New York

69. Lin H, Freeman BD (2005) Materials selection guidelines for membranes that remove CO_2 from gas mixtures J Mol Struct 739:57–74